Available online at www.sciencedirect.com
ScienceDirect
Journal of the European Ceramic Society 28 (2008) 2509–2520
www.elsevier.com/locate/jeurceramsoc

Phase equilibria in the TiO_2–$YO_{1.5}$–ZrO_2 system

Tobias A. Schaedler [a,*], Olga Fabrichnaya [b], Carlos G. Levi [a]

[a] *Materials Department, University of California, Santa Barbara, CA 93106-5050, USA*
[b] *Max-Planck-Institut für Metallforschung, Heisenbergstr. 3, D-70569 Stuttgart, Germany*

Received 14 July 2007; received in revised form 10 March 2008; accepted 15 March 2008
Available online 8 May 2008

Abstract

Isothermal sections of the TiO_2–$YO_{1.5}$–ZrO_2 phase diagram at 1300, 1500 and 1600 °C were studied experimentally using pre-alloyed powders prepared by reverse co-precipitation. The thermodynamic parameters for the TiO_2–$YO_{1.5}$ and TiO_2–ZrO_2 binaries were derived from literature data and combined with the recently determined thermodynamic database for the $YO_{1.5}$–ZrO_2 binary to develop a thermodynamic description of the TiO_2–$YO_{1.5}$–ZrO_2 system. Ternary isothermal sections were calculated between 1200 and 1700 °C and agree well with the experimental evidence. A corollary result of this study is a revised phase diagram for the TiO_2–$YO_{1.5}$ binary.

Keywords: TiO_2; Y_2O_3; ZrO_2; Phase equilibria; Thermodynamic modeling

1. Introduction

The $YO_{1.5}$–ZrO_2 binary has been studied widely owing to its important applications in transformation-toughened ceramics, solid oxide fuel cells (SOFCs) and thermal barrier coatings (TBCs), among others. TiO_2 additions to this system have attracted recent interest for two reasons. Tetragonal compositions in the zirconia-rich corner of the TiO_2–$YO_{1.5}$–ZrO_2 system are of interest because of their potential for enhancing the toughness of the standard thermal barrier oxide, namely ZrO_2–7.6 ± 1 mol%$YO_{1.5}$ (7YSZ), by mechanisms that do not rely on the tetragonal-to-monoclinic transformation.[1] Toughening in these cases is proposed to occur by ferroelastic domain switching,[2] where the effect should scale with the tetragonality (c/a) of the structure.[3] The expected benefit is higher durability, especially in situations where erosion is an issue. The combined requirements that the structure be tetragonal and non-transformable upon thermal cycling leads to the selection of compositions that are metastable at the temperatures of interest.[4] It has been found that TiO_2 is one of a small number of dopants that increase the tetragonality of the zirconia solid solution without compromising its phase stability.[1,5] Moreover, suitable co-doping with Y^{3+} and Ti^{4+} yields compositions that do not transform to monoclinic even after decomposition of the metastable solid solution into its equilibrium assemblage of t + c phases.[1]

A second region of interest in the TiO_2–$YO_{1.5}$–ZrO_2 system involves Zr^{4+} substitution for Ti^{4+} in the $Y_2Ti_2O_7$ pyrochlore, leading to a defect-fluorite structure and a substantial increase in ionic conductivity.[6] It has also been suggested that pyrochlore structures in this system can be suitably doped to exhibit predominantly ionic or mixed ionic–electronic conductivity, as demonstrated for $Gd_2(Zr,Ti)_2O_7$,[7] rendering them suitable for electrodes in SOFCs. The overarching goal is to design a SOFC system wherein the electrolyte and electrodes have improved chemical and thermal expansion compatibility relative to current architectures. Of more fundamental interest is the fact that some compositions around the pyrochlore region in the TiO_2–$YO_{1.5}$–ZrO_2 system can be synthesized as amorphous oxides and then evolved into a series of metastable crystalline structures, all with the same composition but different ionic conductivity.[8] This offers unique opportunities to study the effect of structure on conductivity at the same chemical composition, with concomitant benefits to the science base of the underlying mechanisms.

In spite of the technological interest in the TiO_2–$YO_{1.5}$–ZrO_2 system the understanding of its phase equilibria and associated thermodynamic foundation is largely inadequate, especially when issues related to metastability arise as in the previous examples. The system is rather special from a fundamental

* Corresponding author. Tel.: +1 805 893 8390; fax: +1 805 893 8486.
E-mail address: tobias@engineering.ucsb.edu (T.A. Schaedler).

0955-2219/$ – see front matter © 2008 Elsevier Ltd. All rights reserved.
doi:10.1016/j.jeurceramsoc.2008.03.011

perspective because all solid phases may be envisaged as ordered or distorted versions of the fluorite structure characteristic of ZrO_2 at high temperature.[9] As a first step in enhancing the quality of the thermodynamic information on this system, the present work investigates the phase relations in the TiO_2–$YO_{1.5}$–ZrO_2 system by combining experimental studies with thermodynamic calculations.

2. Previous work in the literature

2.1. $YO_{1.5}$–ZrO_2 binary

The $YO_{1.5}$–ZrO_2 diagram has been the subject of extensive work, most recently by Fabrichnaya and Aldinger[10], and is reasonably well established. Tetragonal (t) is the stable form of pure ZrO_2 at the higher temperatures of interest ($\geq$1200 °C) whereas monoclinic (m) is favored at lower temperatures. Addition of Y^{3+} to t-ZrO_2 stabilizes the cubic phase (fluorite, F), because the oxygen vacancies created by the trivalent cation associate preferably with the host Zr^{4+} reducing the oxygen "crowding" around it.[11] The resulting cubic phase is thus a defect fluorite. At lower temperatures the tetragonal phase is similarly stabilized by Y^{3+} addition relative to monoclinic, but the increasing vacancy concentration eventually renders the cubic phase more stable. There is one intermediate phase in this system, δ-$Y_4Zr_3O_{12}$, that disorders to F above 1390 °C.[12] The C-type rare earth oxide structure of $YO_{1.5}$ (bixbyite, B) exhibits significant solubility for ZrO_2 that increases with increasing temperature to ~10% at 1600 °C and ~20% at 2460 °C.[10,13] $YO_{1.5}$ transforms to a hexagonal form at ~2330 °C that melts at 2438 °C.

2.2. TiO_2–ZrO_2 binary

Different phase diagrams have been proposed for the TiO_2–ZrO_2 binary.[14–19] In contrast with the $YO_{1.5}$–ZrO_2 system, the tetragonal phase supersedes the fluorite form with increasing addition of the smaller cation Ti^{4+} so that F is not stable at any composition below ~2300 °C. Tetragonal zirconia (t) can accommodate much more Ti^{4+} in solid solution than Y^{3+}, up to ~20 mol%.[15–17,19] Conversely, TiO_2 (rutile, R) can dissolve up to 10–20 mol% ZrO_2.[19] The temperatures of the invariant reactions involving $ZrTiO_4$, t-$(Zr,Ti)O_2$, rutile and liquid have been determined by different authors at 1700–1900 °C and are consistent with each other. However, there are large differences in the temperature and character of the invariant reaction between fluorite, liquid and t-$(Zr,Ti)O_2$, which is alternatively reported as a metatectic ($F \leftrightarrow t + L$)[17] or a peritectic ($F + L \leftrightarrow t$).[15] The latter study reports an additional invariant reaction between fluorite, liquid and an even higher temperature form of ZrO_2, which is obviously inconsistent with more recent understanding of the phase transformations in ZrO_2.

The region around the intermediate phase $ZrTiO_4$ (Z) is also under debate. There is agreement that above 1200 °C $ZrTiO_4$ exists in the α-PbO_2 structure with complete cation disorder and a substantial solubility range.[15,18–20] Conversely, an ordered zirconium titanate is the equilibrium configuration at low temperatures, but there is disagreement about the exact composition and structure of this phase. McHale et al. suggested that $ZrTi_2O_6$ is the only stable intermediate phase below 1100 °C,[18] but a $Zr_5Ti_7O_{24}$ structure has also been reported at low temperatures.[21,22] The most recent study proposed a $(Zr,Ti)O_2$ solid solution that spans compositions from 42 to 67% TiO_2 depending on pressure and synthesis temperature and includes the compounds $ZrTi_2O_6$, $Zr_5Ti_7O_{24}$ and $ZrTiO_4$.[23] Phase stability calculations predict that disordered $ZrTiO_4$ is not stable at room temperature with respect to the individual oxides ($ZrO_2 + TiO_2$) but becomes so at 980 ± 150 °C.[20] When cooled very slowly the high-temperature disordered phase was reported to undergo a transformation to an incommensurate partially ordered phase at temperatures below 1200 °C and then to a commensurate ordered phase at ~845 °C.[24,25] The kinetics in the intermediate temperature range (800–1200 °C) is very sluggish and Troitzsch and Ellis[19] used CuO and Li_2MoO_4 fluxes to access equilibrium. The phase diagram resulting from these experiments shows two ordered $(Zr,Ti)_2O_4$ phases with different compositions. A nearly stoichiometric $ZrTiO_4$ was identified at the onset of ordering (1130–1080 °C). At 1060 °C and below, the composition of $(Zr,Ti)_2O_4$ is significantly more Ti-rich and the amount of Ti increases with decreasing temperature.[19] The structure of the ordered phase depends on the exact composition of the compound but all ordered phases have the same space group as disordered $ZrTiO_4$.[23,26]

2.3. TiO_2–$YO_{1.5}$ binary

The least amount of information is available on the TiO_2–$YO_{1.5}$ binary. There are two intermediate compounds, Y_2TiO_5 and $Y_2Ti_2O_7$ (pyrochlore, P).[27] The latter apparently does not disorder to fluorite at elevated temperatures, as is common in the zirconate pyrochlores.[28] Neither an order/disorder temperature nor a melting point has been reported for $Y_2Ti_2O_7$. α-Y_2TiO_5 is orthorhombic and is reported to transform to a hexagonal structure (β) at 1330 °C and then to a fluorite-type solid solution at 1520 °C.[27] Similar low- and high-temperature modifications have been reported for Dy_2TiO_5 and Gd_2TiO_5.[29] The only published phase diagram of the TiO_2–$YO_{1.5}$ system[27] exhibits a combined fluorite/pyrochlore solid solution phase field. The authors could not detect a F–P two-phase region and reported that the lattice parameter of these solid solutions changes continuously as a function of composition suggesting a second order transition between these phases. While that is theoretically possible, it is thermodynamically invalid that the three phases fluorite, pyrochlore and β-Y_2TiO_5 meet at one point as proposed in that study.[27] Alternate scenarios are suggested by related binary systems, especially $DyO_{1.5}$–TiO_2 where the trivalent cations have comparable ionic sizes in sixfold coordination (90 pm for Y^{3+} and 91 pm for Dy^{3+}). The $DyO_{1.5}$–TiO_2 system exhibits similar α + P and β + P fields but also a F + P field above 1680 °C.[29]

2.4. TiO_2–$YO_{1.5}$–ZrO_2 ternary

The TiO_2–$YO_{1.5}$–ZrO_2 ternary phase diagram has not been thoroughly studied before. Yokokawa et al.[30] calcu-

lated an isothermal section at 1300 °C using thermodynamic data from the ZrO_2 literature and estimates for the other oxides based on correlations between interaction parameters and ionic radii. An experimental diagram at 1500 °C published subsequently[31] exhibits significant differences with the calculated version. Notably, it suggests a two-phase field between $Y_2Ti_2O_7$ pyrochlore and $ZrTiO_4$ that is absent in the calculated Diagram.[30] Moreover, the experimental diagram shows some features inconsistent with the phase rule.

Diagrams depicting the phase evolution in precursor-derived mixed oxides after relatively short exposures at various temperatures have been reported by Kobayashi et al.[32] While these are unlikely to represent equilibrium, the diagram drawn after heat treatments of 10 h at 1500 °C provides insight. It shows a rutile + fluorite two-phase field similar to the calculated diagram[30] but inconsistent with the experimental findings by Feighery et al.[31] The diagram also shows the ternary fluorite field extending down to the TiO_2–$YO_{1.5}$, in contrast with the other reported ternaries.[30,31]

Two partial diagrams have been published for the ZrO_2-rich corner of this system at 1500[33] and 1450 °C.[34] Both diagrams report a similar maximum solubility of $YO_{1.5}$ and TiO_2 in tetragonal zirconia (∼12% TiO_2 and 6% $YO_{1.5}$) and a F + t + Z three-phase field. While the phase fields agree qualitatively with the other experimental diagrams,[31,32] the location of the phase boundaries varies considerably.

A comprehensive study combining experimental and modeling work has been undertaken to clear up the ambiguities in this system and establish reliable phase diagrams at 1300–1600 °C. This paper is a first step in that effort. Emphasis was put on the areas around tetragonal ZrO_2 and $Y_2Ti_2O_7$ due to technological interest in compositions of this range for TBC and SOFC applications.

3. Experimental studies

3.1. Synthesis and characterization

Synthesis of powders was carried out by reverse co-precipitation using titanium *iso*-propoxide, yttrium nitrate and zirconium *n*-butoxide (all from Strem Chemicals, Newburyport, MA) as precursors. The precursors were mixed by dissolution in isopropanol (HPLC grade) to achieve the desired compositions. The mix was then slowly added to an aqueous ammonium hydroxide solution that was kept at pH 10 by concurrent addition of concentrated NH_4OH throughout the process. The resulting precipitates were filtered, dried on a hotplate, ground with mortar and pestle and pyrolyzed at 700 °C for 1 h. Pellets were pressed and heat treated in air to investigate the phase equilibrium. The heating and cooling rates were 10 °C/min unless noted otherwise. The phases present were characterized by X-ray diffraction (XRD) (Philips X'pert powder diffractometer). Analytical transmission electron microscopy (TEM) was performed in a JEOL 2010 equipped with an energy dispersive X-ray (EDX) detector (Si-Li, Vantage, Noran Instruments). Standards were used to calibrate the EDX and the accuracy is assumed to be around ±1%. To verify the accuracy of the synthesis method, which has already been proven in other systems, three samples were submitted to an external laboratory (Dirats, Westfield, MA) for quantitative chemical analysis by inductively coupled plasma emission spectrometry. For a sample with nominal composition $Y_2Ti_{0.6}Zr_{1.4}O_7$ (15Ti–50Y–35Zr),[1] the analysis revealed a composition of 50.26Y, 14.93Ti, 33.9Zr with low levels of impurities (0.41Hf, 0.35Al, 0.11Si and 0.042Ca). The Zr precursor contained 1.2% Hf, which is a naturally occurring impurity in zirconia minerals and difficult to separate. The small amount of alumina impurity is probably the result of using alumina crucibles as well as an alumina mortar and pestle.

3.2. TiO_2–$YO_{1.5}$ binary

The XRD results after high-temperature equilibration are summarized in Table 1. To examine the possibility of phase transformations upon cooling the 1500 °C samples were re-heated after characterization to the same temperature, held for 10 h and "quenched" by removing them from the furnace to cool in air in the crucibles. No significant differences were observed in the XRD scans after quenching compared with the samples cooled at 10 °C/min. The sample 25Y–75Ti did not show any signs of partial melting after 10 h at 1560 °C but was fully molten after 10 h at 1600 °C. The observation is consistent with the proposed eutectic at 1580 °C and ∼80%TiO_2 in the literature.[27]

3.3. TiO_2–$YO_{1.5}$–ZrO_2 ternary

The XRD results after high-temperature equilibration are summarized in Table 2. Most of the compositions were selected and synthesized to investigate the phase evolution in this system, discussed elsewhere.[9,35] Additional compositions were identified for equilibration to strategically complete the ternary phase diagram at 1300 °C. Of this collection of samples the pertinent compositions were heat treated at 1500 and 1600 °C to establish isothermal sections at these temperatures.

High-temperature XRD was performed on samples of 20Ti–50Y–30Zr and 30Ti–50Y–20Zr at temperatures up to 1400 °C in air to ascertain that both compositions were pyrochlore at this temperature and no phase transformations (e.g. ordering) occurred during cooling. The samples 10Ti–3Y–87Zr and 10Ti–10Y–80Zr exhibited monoclinic phase at room temperature, consistent with the transformation of a higher temperature tetragonal phase upon cooling below the $T_0^{t/m}$ surface. TEM samples were prepared from selected samples after isothermal heat treatments at 1300 °C to perform quantitative analysis by EDX. It is assumed that the samples had reached their respective equilibrium configurations at 1300 °C and the measurements on neighboring regions of different composition represent those of the phases at the end of tie lines or the corners of three-phase triangles at the temperature of interest. The EDX results are summarized in Table 3. Com-

[1] To facilitate their location on the phase diagram, the compositions are labeled using cation mole percent throughout this paper.

Table 1
XRD results for binary TiO_2–$YO_{1.5}$ samples after isothermal treatments

Heat treatment	10Ti–90Y	18Ti–82Y	25Ti–75Y	33Ti–67Y	40Ti–60Ti	55Ti–45Y	75Ti–25Y
1300 °C/150 h	B + α	B + α	B + α	α	P + α	P + R	R + P
1400 °C/150 h	B + F	B + F + α	F + B + α	β + α + F	–	–	–
1500 °C/150 h	B + F	F + B	F + B	β + F(+α)	–	–	–
1530 °C/10 h	B + F	F + B	F (+B)	P + β	–	–	R + P
1560 °C/110 h	B + F	F + B	F	P	P	–	R + P
1600 °C/10 h	B + F	F + B	F	P	P	–	L

Key: B = bixbyite; F = fluorite; L = molten; P = pyrochlore; R = rutile; α/β = α/β-Y_2TiO_5. The phase listed first is always the most significant in the XRD pattern followed by the second-most significant. Hardly detectable phases are in brackets. (–) = heat treatment not performed.

bining the XRD and EDX results, as well as information from the binaries, isothermal sections of the TiO_2–$YO_{1.5}$–ZrO_2 system were drawn at 1300, 1500 and 1600 °C (Fig. 1). The major uncertainty in the higher temperature sections is the location of the fluorite compositions at the corners of the relevant three-phase triangles. Arguably the most significant change with temperature is the form of the equilibrium between the F, R, Z and P phases on cooling from 1500 to 1300 °C (see Section 5).

4. Modeling

4.1. Modeling approach

The Thermo-Calc software (Thermo-Calc, Stockholm, Sweden)[36] was used to assess the thermodynamic parameters in this ternary system by means of the CALPHAD method.[37] Phases stable in the system TiO_2–$YO_{1.5}$–ZrO_2, their designation and the thermodynamic models used for their description are presented in Table 4. Most of the solid phases (fluorite, tetragonal, pyrochlore) are described by the compound energy formalism.[38] The liquid phase is described by the two sublattice ionic liquid model,[38] with the first sublattice filled by cations and the second one filled by anions, vacancies and neutral species. This study does not consider the metal-rich part of the system and vacancies are not included in the liquid description. The liquid is thus described by the formula $(Ti^{+4}, Y^{+3}, Zr^{+4})_P(O^{-2})_Q$, where P and Q are the number of sites on the cation and anion sublattices, respectively. The stoichiometric factors P and Q vary with the composition in order to maintain electroneutrality. The remaining phases ($ZrTiO_4$, Y_2TiO_5 and δ-$Zr_3Y_4O_{12}$) are treated as stoichiometric. Phases of rutile and pyrochlore are modeled with mixing occuring in one sublattice. The Gibbs energy of a solution phase with mixing in two sublattices (i.e. F, T, M, C,

Table 2
XRD results after isothermal high-temperature treatments

	1300 °C	Time (h)	1500 °C	Time (h)	1550 °C	Time (h)	1600 °C	Time (h)
10Ti–3Y–87Zr	m	50						
10Ti–10Y–80Zr	F + m	560	F + m	168	F + m	30	–	–
10Ti–50Y–40Zr	F	400	F	220	–	–	–	–
15Ti–5Y–80Zr	t (+F)	18	t (+F)	100	–	–	t (+F)	50
15Ti–8Y–77Zr	t + F	100	t + F	100				
15Ti–15Y–70Zr	F + t	100	F + t	100	–	–	F	50
15Ti–50Y–35Zr	F + P	360	F	220	–	–	–	–
16Ti–4Y–80Zr	t	100	t	50				
20Ti–20Y–60Zr	P + F + t	368	F	220	F	110	–	–
20Ti–40Y–40Zr	F + P	560	F + P	220	F + P	30	–	–
20Ti–50Y–30Zr	F + P	580	F + P	144	–	–	F + P	24
25Ti–50Y–25Zr	P + F	360	–	–	–	–	–	–
30Ti–20Y–50Zr	P + t(+Z)	230	F + Z + R	220	–	–	L + F	50
30Ti–30Y–40Zr	P + F + t	368	F + P	220	–	–	P + F	50
30Ti–50Y–20Zr	P	300	P + F	100	–	–	P + F	24
30Ti–60Y–10Zr	P	230	–	–	P	110	P	50
32Ti–25Y–43Zr	P + t	50						
40Ti–20Y–40Zr	P + t + Z	360	F + P + R	220	–	–	L	50
40Ti–40Y–20Zr	P + F + t	168	–	–	–	–	–	–
40Ti–50Y–10Zr	P	300	P	100	–	–	P	24
50Ti–10Y–40Zr	Z + P	300	Z + F + R	220	Z + F + R	30	L + F + R	50
50Ti–20Y–30Zr	P + Z	400	P + F + R	220	–	–	L	50
50Ti–30Y–20Zr	P + Z	300	–	–	P + F + R	30	–	
50Ti–40Y–10Zr	P + Z	300	–	–	–	–	–	–
70Ti–20Y–10Zr	P + R + Z	368	–		–	–	L	24
80Ti–10Y–10Zr	P + R + Z	230	R + P + F	220	R + P + F	30	L	50

Key: B = bixbyite; F = fluorite; L = molten; m = monoclinic zirconia; P = pyrochlore; R = rutile; t = tetragonal zirconia; Z = zirconium titanate.

H) is expressed as

$$G = \sum_i \sum_j Y_i^s Y_j^t G_{i,j} + RT \sum_s \alpha_s \sum_i Y_i^s \ln Y_i^s + \Delta G^{\text{ex}} \quad (1)$$

where Y_i^s is the mole fraction of a constituent i in sublattice s, $G_{i,j}$ is Gibbs energy of a compound formed from species i and j, α_s is the number of sites on the sublattice s/mole of formula units of phase and ΔG^{ex} is the excess Gibbs energy of mixing expressed as

$$\Delta G^{\text{ex}} = \sum_s Y_i^s Y_j^s L_{i,j}^s + \Delta G^{\text{tern}} \quad (2)$$

where

$$L_{i,j}^s = \sum_n (Y_i^s - Y_j^s)^n L_{<MML}^{:MROW>} \quad (3)$$

are the binary interaction parameters in the sublattice s and ΔG^{tern} is the contribution of high-order interactions. As a first approximation, the ternary and quaternary interaction parameters for the solid phases are neglected.

The thermodynamic description for the $YO_{1.5}$–ZrO_2 system from Fabrichnaya et al.[39] is accepted. Thermodynamic parameters for the TiO_2–ZrO_2 and TiO_2–$YO_{1.5}$ system are optimized in the present study using phase equilibria and calorimetric information from the literature as well as phase equilibrium

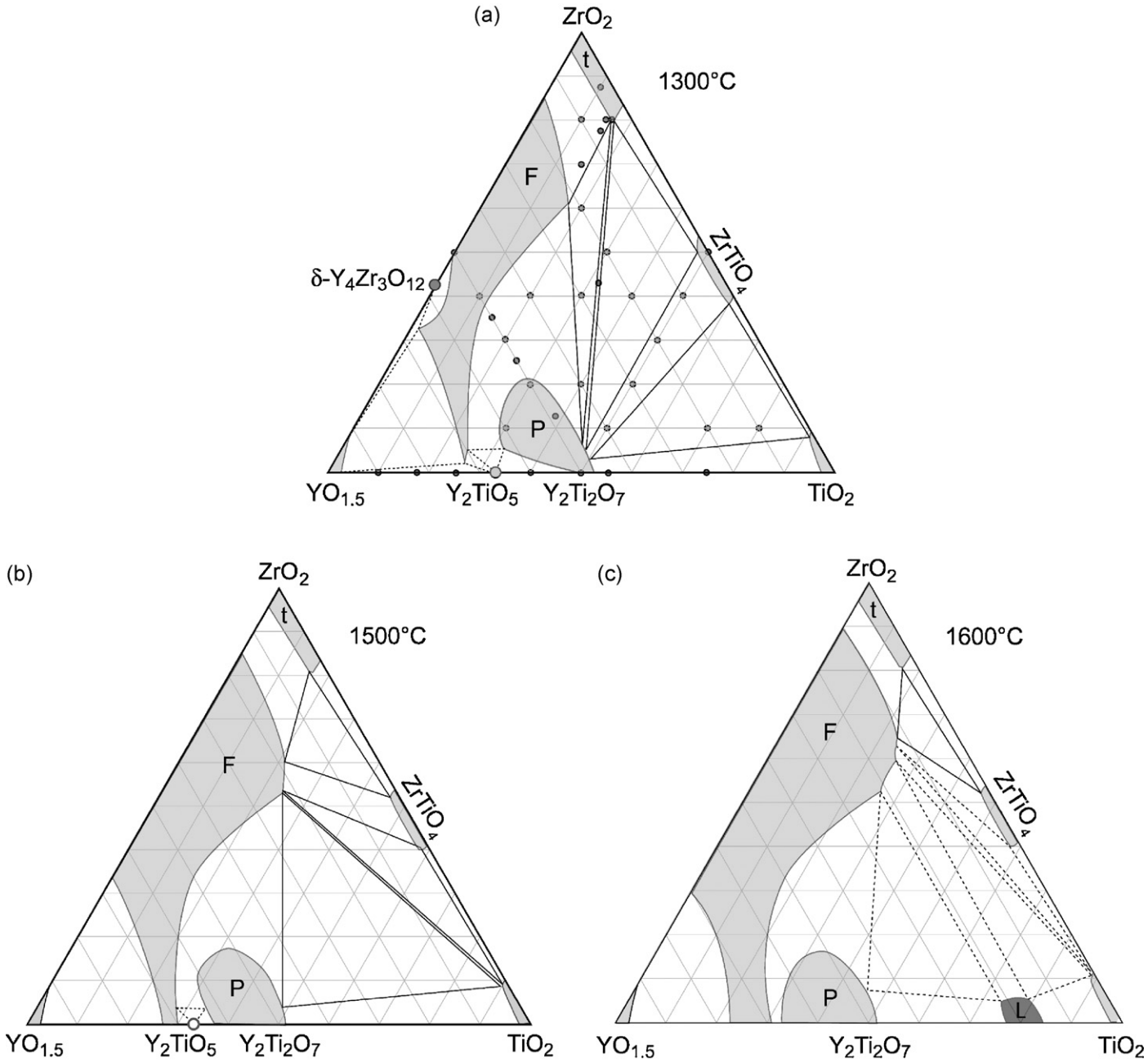

Fig. 1. Isothermal sections of the TiO_2–$YO_{1.5}$–ZrO_2 system based on experimental data: (a) at 1300 °C (compositions equilibrated and characterized are marked), (b) at 1500 °C, (c) at 1600 °C. See Table 2 for detailed XRD results. The dashed lines in the phase diagrams are tentative.

Table 3
Compositions measured by EDX in the TEM

Sample heat treatment	Phase	Composition[a] (at.%)		
		Y	Ti	Zr
20Ti–20Y–60Zr	P	46 ± 1	48 ± 2	6 ± 1
1300 °C/368 h	F	22 ± 1	16	63 ± 1
	t	4 ± 1	16 ± 1	80 ± 1
30Ti–30Y–40Zr	P	46 ± 3	47 ± 2	67 ± 2
1300 °C/368 h	F	22 ± 1	18 ± 1	60 ± 2
	t	5 ± 1	17 ± 1	79 ± 3
40Ti–20Y–40Zr	P	46 ± 3	48 ± 1	5 ± 2
1300 °C/360 h	Z	2 ± 1	50 ± 2	48 ± 2
	t	3 ± 1	16 ± 1	80
80Ti–10Y–10Zr	P	47 ± 1	50 ± 1	4 ± 1
1300 °C/330 h	R	1 ± 1	91 ± 1	8
	Z	2 ± 3	61 ± 4	37 ± 3
20Ti–40Y–40Zr	P	47	45 ± 1	9 ± 1
1300 °C/560 h	F	37 ± 1	13	20 ± 1

[a] The given error corresponds to the standard deviation of measurements on at least four different grains of each phase.

data of the ternary system TiO_2–$YO_{1.5}$–ZrO_2 from the present work. Some simplifications were made in the phase modeling because of uncertainties of the experimental data: $ZrTiO_4$ is considered to be a stoichiometric phase without any ordering. The α ↔ β polymorphic transformation in the Y_2TiO_5 phase is neglected and only the α-phase is considered. The pyrochlore phase, $Y_2(Ti,Zr)_2O_7$, is assumed to be a line compound in the TiO_2–$YO_{1.5}$ system that extends as a planar solid solution field into the ternary system. Thus, disordering in the Y sublattice as well as in the anionic sublattice in the pyrochlore phase is neglected. The assessed thermodynamic parameters of the TiO_2–$YO_{1.5}$–ZrO_2 system are presented in Table 4.

4.2. Calculated TiO_2–$YO_{1.5}$ binary

The calculated phase diagram of the TiO_2–$YO_{1.5}$ system is presented in Fig. 2a. The thermodynamic parameters were assessed using phase equilibrium data from this work and Mizutani et al.[27] as well as calorimetric data for the enthalpy of formation of the $Y_2Ti_2O_7$ phase.[40] The optimizing parameters were the entropy of formation of $Y_2Ti_2O_7$, the enthalpy and entropy of formation of Y_2TiO_5 and the mixing parameters in the fluorite phase. Since several simplifications were made in the phase modeling, it was not possible to get a better fit of the experimental data. However, it should be mentioned that the important features of the experimental phase diagram are reproduced in the calculations. The experimental determination of the $Y_2Ti_2O_7$ melting point would be important information to improve the thermodynamic description of the TiO_2–$YO_{1.5}$ system. Combining the experimental and modeling results (melting point of $Y_2Ti_2O_7$ and liquidus) of this study, as well as input from the previously published binary[27] a tentative phase diagram has been drawn for the TiO_2–$YO_{1.5}$ system and is depicted in Fig. 2b.

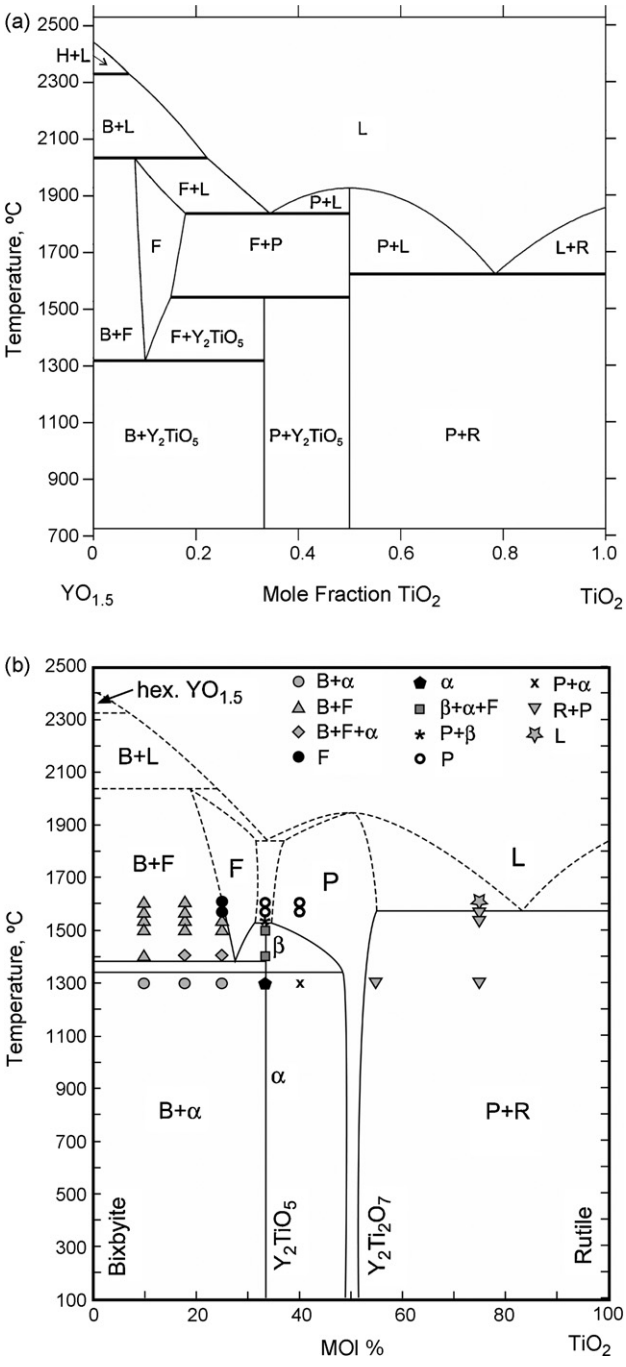

Fig. 2. (a) Calculated phase diagram of the TiO_2–$YO_{1.5}$ system. (b) Phase diagram of the TiO_2–$YO_{1.5}$ system combining modeling results and experimental results (marked), as well as information from the previously published version[27] (dashed lines are tentative).

4.3. Calculated TiO_2–ZrO_2 binary

The thermodynamic parameters of the TiO_2–ZrO_2 system are available in work of Cancarevic et al.[41] However, the associate model for liquid and solid solutions applied in the cited work is incompatible with ionic liquid model and compound energy formalism used in the present work. Therefore, a new description of the TiO_2–ZrO_2 system was derived. The first assessment of the thermodynamic parameters was based on experimental

Table 4
Thermodynamic parameters for phases in the TiO_2–Y_2O_3–ZrO_2 system

Phase, temperature range	Model/parameter
IONIC_LIQUID (L), 298.15–4000	$(Ti^{+4},Y^{+3},Zr^{+4})(O^{-2})_2$ $G(IONIC\_LIQUID,Ti^{+4}:O^{-2}) = 2\cdot GTIO2 + 134571.01 - 62.477\cdot T$ $G(IONIC\_LIQUID,Zr^{+4}:O^{-2}) = 2\cdot GZRO2L$ $G(IONIC\_LIQUID,Y^{+3}:O^{-2}) = 2\cdot GYYLIQ + 3\cdot GHSEROO - 1821322.19 + 243.52552\cdot T$ $G(IONIC\_LIQUID,Ti^{+4},Zr^{+4}:O^{-2}) = -35000$ $^0L(IONIC\_LIQUID,Y^{+3},Zr^{+4}:O^{-2}) = 11488.4008$ $^1L(IONIC\_LIQUID,Y^{+3},Zr^{+4}:O^{-2}) = 1608.38521$ $^0L(IONIC\_LIQUID,Ti^{+4},Y^{+3}:O^{-2}) = -150000$
Y_2O_3_CUBIC (B), 298.15–6000	$(Y^{+3},Zr^{+4})_2\ (O^{-2})_3\ (O^{-2},Va)$ $G(Y2O3\_CUB,Zr^{+4}:O^{-2}:O^{-2}) = 2\cdot GZRO2C$ $G(Y2O3\_CUB,Zr^{+4}:O^{-2}:Va) = 2\cdot GZRO2C - GHSEROO$ $G(Y2O3\_CUB,Y^{+3}:O^{-2}:O^{-2}) = GY2O3R + GHSEROO$ $G(Y2O3\_CUB,Y^{+3}:O^{-2}:Va) = +GY2O3R$ $^0L(Y2O3\_CUB,Y^{+3},Zr^{+4}:O^{-2}:O^{-2}) = -34451.2175 + 39.5035342\cdot T$ $^0L(Y2O3\_CUB,Y^{+3},Zr^{+4}:O^{-2}:Va) = -34451.2175 + 39.5035342\cdot T$
Y_2O_3_HEXAGONAL (H), 298.15–6000	$(Y^{+3},Zr^{+4})_2\ (O^{-2})_3\ (O^{-2},Va)$ $G(Y2O3\_HEX,Zr^{+4}:O^{-2}:O^{-2}) = 2\cdot GZRO2C + 50000$ $G(Y2O3\_HEX,Zr^{+4}:O^{-2}:Va) = 2\cdot GZRO2C - GHSEROO + 50000$ $G(Y2O3\_HEX,Y^{+3}:O^{-2}:O^{-2}) = GY2O3H + GHSEROO$ $G(Y2O3\_HEX,Y^{+3}:O^{-2}:Va) = GY2O3H$ $^0L(Y2O3\_HEX,Y^{+3},Zr^{+4}:O^{-2}:O^{-2}) = 180000$ $^0L(Y2O3\_HEX,Y^{+3},Zr^{+4}:O^{-2}:Va) = 180000$
RUTILE (R), 298.15–6000	$(Ti^{+4},Zr^{+4})(O^{-2})_2$ $G(RUTILE,Ti^{+4}:O^{-2}) = GTIO2 + 747.5$ $G(RUTILE,Zr^{+4}:O^{-2}) = GZRO2C + 43000$
ZrO_2_FLUORITE (F), 298.15–6000	$(Ti^{+4},Y^{+3},Zr^{+4})\ (O^{-2},Va)_2$ $G(ZRO2\_FLU,Zr^{+4}:O^{-2}) = GZRO2C$ $G(ZRO2\_FLU,Zr^{+4}:Va) = GZRO2C - 2\cdot GHSEROO$ $G(ZRO2\_FLU,Ti^{+4}:O^{-2}) = GTIO2 + 25000$ $G(ZRO2\_FLU,Ti^{+4}:Va) = GTIO2 - 2\cdot GHSERO + 25000$ $G(ZRO2\_FLU,Y^{+3}:O^{-2}) = 0.5\cdot GY2O3R + 2000 + 0.5\cdot GHSEROO + 9.3511\cdot T$ $G(ZRO2\_FLU,Y^{+3}:Va) = 0.5\cdot GY2O3R + 2000 - 1.5\cdot GHSEROO + 9.3511\cdot T$ $^0L(ZRO2\_FLU,Y^{+3},Zr^{+4}:O^{-2}) = -65401.3858 + 25.099522\cdot T$ $^0L(ZRO2\_FIU,Y^{+3},Zr^{+4}:Va) = -65401.3858 + 25.099522\cdot T$ $^1L(ZRO2\_FLU,Y^{+3},Zr^{+4}:O^{-2}) = 67041.1965 - 21.0271896\cdot T$ $^1L(ZRO2\_FLU,Y^{+3},Zr^{+4}:Va) = 67041.1965 - 21.0271896\cdot T$ $^0L(ZRO2\_FLU,Ti^{+4},Y^{+3}:O^{-2}) = -54000.0$ $^0L(ZRO2\_FLU,Ti^{+4},Y^{+3}:Va) = -54000.0$
ZrO_2_TETRAGONAL (t), 298.15–6000	$(Ti^{+4},Y^{+3},Zr^{+4})\ (O^{-2},Va)_2$ $G(ZRO2\_TETR,Zr^{+4}:O^{-2}) = GZRO2T$ $G(ZRO2\_TETR,Zr^{+4}:Va) = GZRO2T - 2\cdot GHSEROO$ $G(ZRO2\_TETR,Ti^{+4}:O^{-2}) = GTIO2 + 17000$ $G(ZRO2\_TETR,Ti^{+4}:Va) = GTIO2 - 2\cdot GHSEROO + 17000$ $G(ZRO2\_TETR,Y^{+3}:O^{-2}) = 0.5\cdot GY2O3R + 10000 + 0.5\cdot GHSEROO + 9.3511\cdot T$ $G(ZRO2\_TETR,Y^{+3}:Va) = 0.5\cdot GY2O3R + 10000 - 1.5\cdot GHSEROO + 9.3511\cdot T$ $^0L(ZRO2\_TETR,Y^{+3},Zr^{+4}:O^{-2}) = -63233.7083 + 30\cdot T$ $^0L(ZRO2\_TETR,Y^{+3},Zr^{+4}:Va) = -63233.7083 + 30\cdot T$
ZrO_2_MONOCLINIC (m), 298.15–6000	$(Ti^{+4},Y^{+3},Zr^{+4})\ (O^{-2},Va)_2$ $G(ZRO2\_MONO,Zr^{+4}:O^{-2}) = GZRO2M$ $G(ZRO2\_MONO,Zr^{+4}:Va) = GZRO2M - 2\cdot GHSEROO$ $G(ZRO2\_MONO,Ti^{+4}:O^{-2}) = GTIO2 + 40000$ $G(ZRO2\_MONO,Ti^{+4}:Va) = GTIO2 - 2\cdot GHSERO + 40000$ $G(ZRO2\_MONO,Y^{+3}:O^{-2}) = 0.5\cdot GY2O3R + 26900 + 0.5\cdot GHSEROO + 25.4\cdot T + 9.3511\cdot T$ $G(ZRO2\_MONO,Y^{+3}:Va) = 0.5\cdot GY2O3R + 26900 - 1.5\cdot GHSEROO + 25.4\cdot T + 9.3511\cdot T$
PYROCHLORE (P), 298.15–6000	$(Y^{+3})_2(Ti^{+4},Zr^{+4})_2(O^{-2})_7$ $G(PYROCHLORE,Y^{+3}:Ti^{+4}:O^{-2}) = GYTIO$ $G(Y2TI2O7,Y^{+3}:Zr^{+4}:O^{-2}) = 2\cdot GZRO2C + GY2O3R + 2000$
Y_2TiO_5 (α), 298.15–6000	$(Y^{+3})_2(Ti^{+4})(O^{-2})_5$ $G(Y2TIO5,Y^{+3}:Ti^{+4}:O^{-2}) = GY2O3R + GTIO2 + 747.5 - 74324 + 11.21\cdot T$

Table 4 (*Continued*)

Phase, temperature range	Model/parameter
$Zr_3Y_4O_{12}$ (δ), 298.15–6000	$(Zr^{+4})_3(Y^{+3})_4(O^{-2})_{12}$ $G(ZR3Y4O12,Zr^{+4}:Y^{+3}:O^{-2}) = 7\cdot GZYO$
$ZrTiO_4$ (Z), 298.15–6000	$(Zr^{+4})(Ti^{+4})(O^{-2})_4$ $G(ZRTIO4,Zr^{+4}:Ti^{+4}:O^{-2}) = GZRTIO4$

Temperature range	Functions
298.15–900	$GHSERTI = -8059.921 + 133.615208\cdot T - 23.9933\cdot T\cdot\ln(T) - 0.004777975\cdot T^2 + 1.06716\cdot10^{-7}\cdot T^3 + 72636/T$
900–1155	$-7811.815 + 132.988068\cdot T - 23.9887\cdot T\cdot\ln(T) - 0.0042033\cdot T^2 - 9.0876\cdot10^{-8}\cdot T^3 + 42680/T$
1155–1940.99	$+908.837 + 66.976538\cdot T - 14.9466\cdot T\cdot\ln(T) - 0.0081465\cdot T^2 + 2.02715\cdot10^{-7}\cdot T^3 - 1477660/T$
1940.99–4000	$-124526.786 + 638.806871\cdot T - 87.2182461\cdot T\cdot\ln(T) + 0.008204849\cdot T^2 - 3.04747\cdot10^{-7}\cdot T^3 + 36699805/T$
298.15–1000	$GHSEROO = -3480.87 - 25.503038\cdot T - 11.1355\cdot T\cdot\ln(T) - 0.005098875\cdot T^2 + 6.61845833\cdot10^{-7}\cdot T^3 - 38365/T$
1000–3300	$-6568.763 + 12.659879\cdot T - 16.8138\cdot T\cdot\ln(T) - 5.957975\cdot10^{-4}\cdot T^2 + 6.781\cdot10^{-9}\cdot T^3 + 262905/T$
3300–6000	$-13986.728 + 31.259624\cdot T - 18.9536\cdot T\cdot\ln(T) - 4.25243\cdot10^{-4}\cdot T^2 + 1.0721\cdot10^{-8}\cdot T^3 + 4383200/T$
298.15–1000	$GHSERYY = -8011.09379 + 128.572856\cdot T - 25.6656992\cdot T\cdot\ln(T) - 0.00175716414\cdot T^2 - 4.17561786\cdot10^{-7}\cdot T^3 + 26911.509/T$
1000–1795.15	$-7179.74574 + 114.497104\cdot T - 23.4941827\cdot T\cdot\ln(T) - 0.0038211802\cdot T^2 - 8.2534534\cdot10^{-8}\cdot T^3$
1795.15–3700	$-67480.7761 + 382.124727\cdot T - 56.9527111\cdot T\cdot\ln(T) + 0.00231774379\cdot T^2 - 7.22513088\cdot10^{-8}\cdot T^3 + 18077162.6/T$
298.15–2128	$GHSERZR = -7827.595 - 125.64905\cdot T - 24.1618\cdot T\cdot\ln(T) - 0.00437791\cdot T^2 + 34971/T$
2128–6000	$-26085.921 + 2622.724183\cdot T - 42.144\cdot T\cdot\ln(T) - 1.342895\cdot10^{-31}\cdot T^{-9}$
298.15–900	$GTILIQ = 12194.415 - 6.980938\cdot T + GHSERTI$
900–1300	$+12194.416 - 6.980938\cdot T + GHSERTI$
1300–1940.99	$+369519.198 - 2554.0225\cdot T + 342.059267\cdot T\cdot\ln(T) - 0.163409355\cdot T^2 + 1.2457117\cdot10^{-5}\cdot T^3 - 67034516/T$
1940.99–4000	$-19887.066 + 298.7367\cdot T - 46.29\cdot T\cdot\ln(T)$
298.15–700	$GTIO2 = -966880.637 + 528342.968/T + 348.553335\cdot T - 57.0208072\cdot T\cdot\ln(T) - 0.0201717125\cdot T^2 + 3.85969119\cdot10^{-6}\cdot T^3$
700–2130	$-974253.518 + 1126926.93/T + 461.205243\cdot T - 74.5187136\cdot T\cdot\ln(T) - 0.00135696952\cdot T^2 + 2.10166504\cdot10^{-8}\cdot T^3$
2130–6000	$-1022606.35 + 679.833124\cdot T - 100.416\cdot T\cdot\ln(T)$
298.15–2985	$GZRO2M = -1126367.62 + 426.0761\cdot T - 69.6218\cdot T\cdot\ln(T) - 0.0037656\cdot T^2 + 702910/T$
2986–6000	$-1145443.9237 + 567.31299\cdot T - 87.864\cdot T\cdot\ln(T) - 2.54642\cdot10^{33}\cdot T^{-9}$
298.15–1478	$GZRO2T = -1117868.813 + 420.27778\cdot T - 69.6218\cdot T\cdot\ln(T) - 0.0037656\cdot T^2 + 702910.0/T + 4.589486\cdot10^{-21}\cdot T^7$
1478–2985	$-1121646.51 + 479.515703\cdot T - 78.10\cdot T\cdot\ln(T)$
2985–6000	$-1154030.428 + 568.38136\cdot T - 87.864\cdot T\cdot\ln(T) + 6.092955\cdot10^{33}\cdot T^{-9}$
298.15–1800	$GZRO2C = -1107276.18 + 416.6337865\cdot T - 69.6218\cdot T\cdot\ln(T) - 0.0037656\cdot T^2 + 702910.0/T + 1.920919\cdot10^{-21}\cdot T^7$
1800–2985	$-1113681 + 491.486437\cdot T - 80.0\cdot T\cdot\ln(T)$
2985–6000	$-1139763.268 + 563.059458\cdot T - 87.864\cdot T\cdot\ln(T) + 4.90732\cdot10^{33}\cdot T^{-9}$
298.15–2985	$GZRO2L = -1027958.268 + 390.79315\cdot T - 69.6218\cdot T\cdot\ln(T) - 0.0037656\cdot T^2 + 702910/T + 1.373457\cdot10^{-22}\cdot T^7$
2985–6000	$-1050128.04 + 533.11826\cdot T - 87.864\cdot T\cdot\ln(T)$
298.15–1000	$GYYLIQ = 2098.50738 + 119.41873\cdot T - 24.6467508\cdot T\cdot\ln(T) - 0.00347023463\cdot T^2 - 8.12981167\cdot10^{-7}\cdot T^3 + 23713.7332/T$
1000–1795.15	$+7386.44846 + 19.4520171\cdot T - 9.0681627\cdot T\cdot\ln(T) - 0.0189533369\cdot T^2 + 1.7595327\cdot10^{-6}\cdot T^3$
1795.15–3700	$-12976.5957 + 257.400783\cdot T - 43.0952\cdot T\cdot\ln(T)$
298.15–6000	$GY2O3R = -1984291 + 763.71851\cdot T - 125.692\cdot T\cdot\ln(T) - 0.00558\cdot T^2 + 2344020.5/T - 117305560/T^2$
298.15–6000	$GY2O3H = -1959291 + 754.10313\cdot T - 125.692\cdot T\cdot\ln(T) - 0.00558\cdot T^2 + 2344020.5/T - 117305560/T^2$
298.15–6000	$GZYO = 0.4286\cdot GZRO2C + 0.2857\cdot GY2O3R - 14550.3912 - 0.520412688\cdot T$
298.15–6000	$GYTIO = GY2O3R + 2\cdot GTIO2 + 1495 - 86200 - 10.0\cdot T$
298.15–6000	$GZRTIO4 = -2075176.9 + 793.557\cdot T - 132.455473\cdot T\cdot\ln(T) - 0.0160526739\cdot T^2 + 1222219.12/T + 1.74275446\cdot10^{-9}\cdot T^4$ $- 2.7368539\cdot10^{-16}\cdot T^6 + 2.64004889\cdot10^{-23}\cdot T^8 - 1.00223393\cdot10^{-30}\cdot T^{10}$

phase equilibrium data[14–18] and the Gibbs energy expression for the $ZrTiO_4$ phase based on calorimetric measurements and calculations from vibrational spectra.[20] The optimized parameters were the Gibbs energies of fictive end-members (TiO_2 with structures of fluorite, tetragonal and monoclinic phase and ZrO_2 with the rutile structure) and the mixing parameter of the liquid phase. When using the initially derived parameters in the ternary system TiO_2–$YO_{1.5}$–ZrO_2 it was found that the Gibbs energy of $ZrTiO_4$ should be 2 kJ more negative to reproduce the experimental tie lines at 1300 °C determined in the present investigation. This motivated a reassessment of the mixing parameter of the liquid in the TiO_2–ZrO_2 binary using the modified Gibbs energy of the $ZrTiO_4$ phase. The calculated phase diagram of the TiO_2–ZrO_2 binary is presented in Fig. 3. The results are in reasonable agreement with experimental data in the literatures[15–17] and reproduce the solid solubility of TiO_2 in the tetragonal phase proposed by other authors.[15,17,19] The calculated solid solubility of ZrO_2 in the rutile structure is less than that reported from experiments.[14–19] The calculated data for the reaction T ↔ F + L is consistent with the results of Noguchi and Mizuno[15], but not of

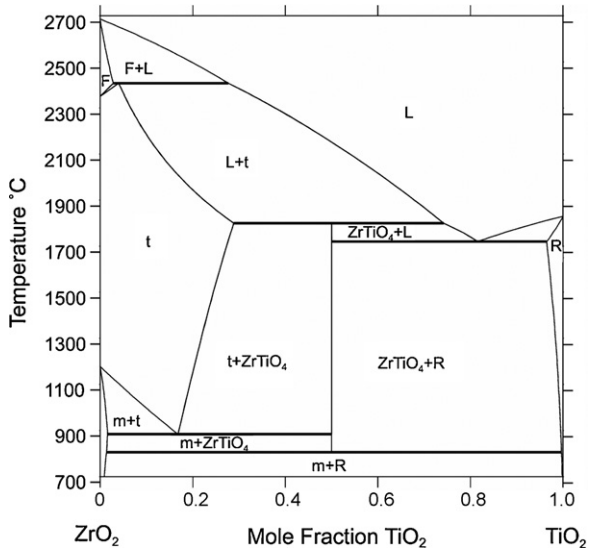

Fig. 3. Calculated phase diagram of the TiO_2–ZrO_2 system.

Shevchenko et al.[17] (It should be mentioned that in both experimental works this invariant reaction was shown tentatively.) The diagram is also in qualitative agreement with an earlier calculation by Yokokawa et al.[30] but the latter shows the invariant reaction as proposed by Shevchenko et al.[17]

4.4. Calculated TiO_2–$YO_{1.5}$–ZrO_2 isothermal sections

Isothermal sections for the TiO_2–$YO_{1.5}$–ZrO_2 system were calculated at various temperatures between 1000 and 1700 °C and are presented in Fig. 4. Isothermal sections at temperatures below 1000 °C were not calculated because the ordered phase with a composition of ~60% TiO_2 occurring below 1050 °C[19] in the TiO_2–ZrO_2 system was not included in the model. Two transitional (übergang) reactions were calculated between the low temperature equilibria and the onset of melting:

$$F + Z \Leftrightarrow P + t \qquad (1399\,^{\circ}C)$$

$$Z + P \Leftrightarrow F + R \qquad (1596\,^{\circ}C)$$

Both reactions are observed experimentally between 1300 and 1500 °C. It should be noted that the reactions were first obtained in calculations and then experimentally confirmed. However, not all experimental data are quantitatively reproduced by calculations. The calculated fluorite phase field is significantly smaller than experimentally observed, and the predicted temperature of one of the reactions above is higher than determined experimentally. One possible reason is the simplification in the modeling of the fluorite structure. In reality the defect-fluorite structure comprised of different cations and oxygen vacancies can lower its free energy by adopting various degrees of local order.[42,43]

5. Discussion

5.1. The TiO_2–$YO_{1.5}$ binary

The results of the long-term isothermal heat treatments are in good agreement with the phase diagram by Mizutani et al.,[27] but there is an important discrepancy between them and the calculated diagram in Fig. 2a. This is the absence of clear experimental evidence for a binary P + F two-phase field. Since such field exists in the ternary (Fig. 1) and both phases exist in the binary, the P + F field is expected to extend to the binary. This prohibits the existence of a higher order pyrochlore to fluorite phase transformation as suggested by Mizutani et al.[27] The composition 66.7Y–33.3Ti (Y_2TiO_5) formed single-phase pyrochlore above 1560 °C. If there was a two-phase field of significant "width", peak splitting into fluorite and pyrochlore XRD reflections would be expected due to different lattice parameters, as seen in ternary compositions in the P + F field.[9] However, if the compositions of the fluorite and pyrochlore phases are similar, the XRD reflections of the fluorite phase could be "hiding" under the reflections of the pyrochlore phase. Compositional inaccuracies of the 66.7Y–33.3Ti sample can be ruled out since its composition was verified by an external laboratory. Considering the modeling results and rules for the construction of phase diagrams, the Y_2TiO_5 phase is expected to lead into the P + F field above ~1500 °C and the absence of experimental evidence of the fluorite phase could be contributed to the "narrowness" of this two-phase field and to the composition 66.7Y–33.3Ti being very close to the pyrochlore phase field, as indicated in Fig. 2b. The appearance of fluorite as a second phase in 66.7Y–33.3Ti at 1400 and 1500 °C is unprecedented. The small amounts of α-phase after heat treatments at these temperatures could be due to incomplete α–β phase transformation or due to formation of α-phase upon cooling. In Fig. 2b the experimental and modeling results have been combined to draw a new tentative version of the phase diagram. The phase equilibria involving the β-phase could not be completely resolved within this study (the crystal structure of the β-phase has not been solved, either).

5.2. Isothermal sections of the TiO_2–$YO_{1.5}$–ZrO_2 system

The general features of the calculated diagram at 1300 °C in Fig. 4c are in good agreement with the experimental diagram in Fig. 1a. EDX was performed on two samples in the P + F + t field (samples 20Ti–20Y–60Zr and 30Ti–30Y–40Zr) and the averages of the measured values were used to determine the compositions of the phases at the corner of the triangle, namely 48Ti–45Y–7Zr (P), 17Ti–22Y–61Zr (F) and 16Ti–4Y–80Zr (t). The values for the tetragonal phase are very similar to the composition for the same phase measured in the 40Ti–20Y–40Zr sample, which falls on the P + Z + t field, indicating that both three-phase fields meet near the ternary corner of the tetragonal phase field, and the P + t two-phase field between them is very narrow. Analysis of 16Ti–4Y–80Zr and 15Ti–5Y–80Zr samples annealed at temperatures between 1300 and 1600 °C (Table 2) confirmed the identity of the former as the ternary solubility limit for the tetragonal phase and its small depen-

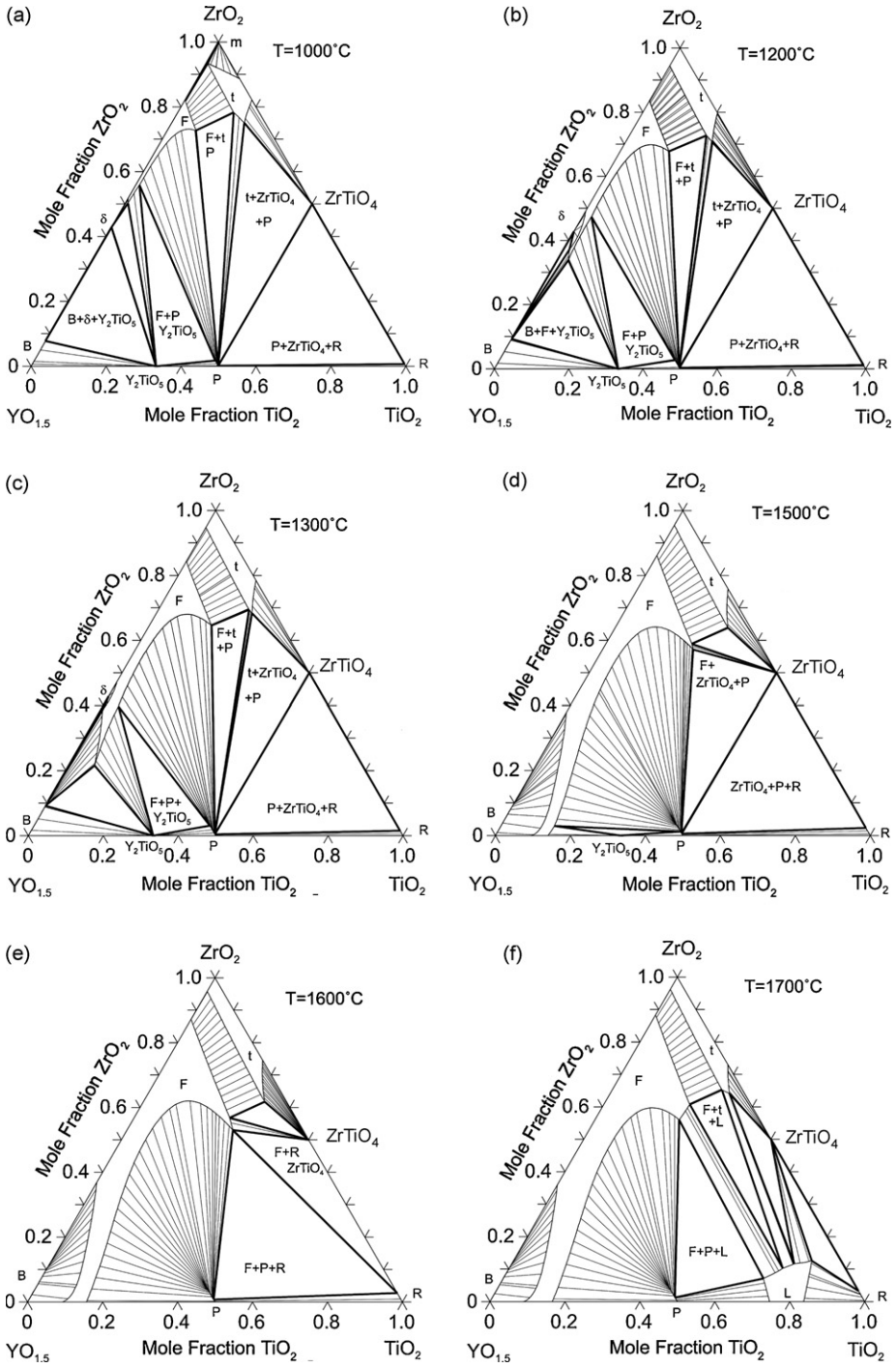

Fig. 4. Calculated isothermal sections of the TiO_2–$YO_{1.5}$–ZrO_2 system: (a) at 1000 °C, (b) at 1200 °C, (c) at 1300 °C, (d) at 1500 °C, (e) at 1600 °C, (f) at 1700 °C.

dence on temperature within this range (Fig. 1). The width of the P + F two-phase field along the 50Y isoconcentrate is in good agreement with the compositions reported by Liu et al.[44] for a sample of 20Ti–50Y–30Zr equilibrated at 1350 °C, i.e. 23Ti–50Y–27Zr (F) and 16Ti–50Y–34Zr (P). The solid solubility of $ZrTiO_4$ in the ternary at 1500 °C (Fig 1b) is reported by McHale and Roth[18] as ranging from 45 to 58%TiO_2 at 1% Y. The reported solubility range in the binary suggests that the width of this field is relatively insensitive to temperature, as reflected in Fig. 1a–c.

The calculated diagram at 1500 °C fits the experimental one reasonably well, except that the model predicts the invariant reaction $Z + P \leftrightarrow F + R$ to occur at 1596 °C whereas the experiments reveal it takes place at 1500 °C. The Ti-rich samples showed partial melting between 1560 and 1600 °C, which resulted in the pellets bonding to the crucibles. The behavior is consistent with the reported eutectic in the TiO_2–$YO_{1.5}$ binary at 1580 °C and ~82% TiO_2.[27] Based on the existence of eutectics on both binary sides of the rutile field, one might anticipate that incipient melting for the ternary compositions is

below 1580 °C. Note, however, that melting is predicted to occur above 1600 °C in the calculated diagram (Fig. 4e and f), with a predicted eutectic at ~1650 °C. In general the thermodynamic model appears to over-predict the temperatures of invariant reactions and requires further refinement to better fit the experimental data. Such refinement, however, requires additional experimental information.

The findings of this work are significant for ceramic technology in two main areas. The large solubility range of the pyrochlore phase field allows exploiting increases in ionic conductivity by replacing up to 20% Ti^{4+} with Zr^{4+} in $Y_2Ti_2O_7$ pyrochlore in equilibrium at 1300 °C.[6,8] Arguably more Zr^{4+} can be substituted extending the solubility metastably, but after longer times at 1300 °C the equilibrium fluorite + pyrochlore two-phase mixture will form. The ability of the $Y_2Ti_2O_7$ pyrochlore structure to tolerate substantial amounts of substitution with Zr^{4+} and presumably similar cations, too, offers opportunity to tailor its electronic and/or ionic conductivity for use in solid oxide fuel cells. Determining the phase boundaries in the zirconia-rich corner of the TiO_2–$YO_{1.5}$–ZrO_2 system is important for assessing the "window of opportunity" for enhancing tetragonality and toughness of YSZ by addition of titania.[1] A maximum of 16% TiO_2 can be substituted for ZrO_2 in 7YSZ while staying within the t + F two-phase field. Single-phase tetragonal zirconia can dissolve a maximum of 4% $YO_{1.5}$ and 16% TiO_2 in equilibrium. Knowledge of these phase boundaries will guide the optimization of compositions of advanced thermal barrier coatings based on titania doped YSZ with respect to toughness, phase stability and thermal conductivity.

6. Summary

The phase equilibria of the TiO_2–$YO_{1.5}$–ZrO_2 system have been examined by experiments and calculations and an understanding has been developed. Ternary phase diagrams were established experimentally at 1300, 1500 and 1600 °C. A thermodynamic description of the TiO_2–$YO_{1.5}$–ZrO_2 system was developed and ternary isothermal sections were calculated between 1200 and 1700 °C. The modeling results agree well with the experimental results. Significant is the existence of two-phase fields between pyrochlore and $ZrTiO_4$ and between pyrochlore and t-ZrO_2 at 1300 °C that were not considered in an earlier version.[39] Two invariant reactions of the transitional type were revealed in calculations and then experimentally confirmed to occur between 1300 and 1500 °C. An effort to model the TiO_2–$YO_{1.5}$ and TiO_2–ZrO_2 binaries has also been undertaken. Combining modeling and experimental results, a revised phase diagram for the TiO_2–$YO_{1.5}$ binary is suggested.

Acknowledgements

This research was financially supported by the National Science Foundation (NSF) under grants DMR-0605700 and DMR-0080021 (subcontract from SUNY-Stony Brook). The work made use of the MRL Central Facilities at UCSB supported by the NSF under Award No. DMR-0520415.

References

1. Schaedler, T. A., Leckie, R. M., Krämer, S., Evans, A. G. and Levi, C. G., Toughening of non-transformable t′-YSZ by addition of titania. *J. Am. Ceram. Soc.*, 2007, **90**, 3896–3901.
2. Virkar, A. V., Role of ferroelasticity in toughening of zirconia ceramics. *Key Eng. Mater.*, 1998, **153**, 183–210.
3. Mercer, C., Williams, J. R., Clarke, D. R. and Evans, A. G., On a ferroelastic mechanism governing the toughness of metastable tetragonal-prime (t′) yttria-stabilized zirconia. *Proc. R. Soc. A*, 2007, **2081**, 1393–1408.
4. Levi, C. G., Emerging materials and processes for thermal barrier systems. *Curr. Opin. Solid State Mater. Sci.*, 2004, **8**, 77–91.
5. Pitek, F. M. and Levi, C. G., Opportunities for TBCs in the ZrO_2–$YO_{1.5}$–$TaO_{2.5}$ system. *Surf. Coat. Technol.*, 2007, **201**, 6044–6050.
6. Wuensch, B. J., Eberman, K. W., Heremans, C., Ku, E. M., Onnerud, P., Yeo, E. M. E., Haile, S. M., Stalick, J. K. and Jorgensen, J. D., Connection between oxygen-ion conductivity of pyrochlore fuel-cell materials and structural change with composition and temperature. *Solid State Ionics*, 2000, **129**, 111–133.
7. Tuller, H. L., Mixed ionic–electronic conduction in a number of fluorite and pyrochlore compounds. *Solid State Ionics*, 1992, **52**, 135–146.
8. Schaedler, T. S., Phase Evolution in the $YO_{1.5}$–TiO_2–ZrO_2 System and Effects on Ionic Conductivity and Toughness. PhD thesis, University of California, Santa Barbara, CA, 2006.
9. Schaedler, T. A., Francillon, W., Gandhi, A. S., Grey, C. P., Sampath, S. and Levi, C. G., Phase evolution in the $YO_{1.5}$–TiO_2–ZrO_2 system around the pyrochlore structure. *Acta Mater.*, 2005, **53**, 2957–2968.
10. Fabrichnaya, O. and Aldinger, F., Assessment of thermodynamic parameters in the system ZrO_2–Y_2O_3–Al_2O_3. *Zeitschrift für Metallkunde*, 2004, **95**, 27–39.
11. Li, P., Chen, I. and Penner-Hahn, J. E., Effects of dopants on zirconia stabilization—an X-ray absorption study. I. Trivalent dopants. *J. Am. Ceram. Soc.*, 1994, **77**, 118–128.
12. Du, Y., Jin, Z. and Huang, P. J., Thermodynamic assessment of the $ZrO_2YO_{1.5}$ system. *J. Am. Ceram. Soc.*, 1991, **74**, 1569–1577.
13. Stubican, V. S., Phase equilibria and metastabilities in the systems ZrO_2–MgO, ZrO_2–CaO and ZrO_2–Y_2O_3. In *Science and Technology of Zirconia III*, ed. S. Somiya, N. Yamamoto and H. Hanagida. The American Ceramic Soc., Columbus, OH, 1988, pp. 71–82.
14. Coughanour, L. W., Roth, R. S. and DeProsse, V. A., Phase equilibrium relations in the system lime–titania and zirconia–titania. *J. Res. Natl. Bur. Stand.*, 1954, **52**, 37–42.
15. Noguchi, T. and Mizuno, M., Phase changes in solids measured in a solar furnace ZrO_2–TiO_2 system. *Sol. Energy*, 1967, **11**, 56–61.
16. Ono, A., *Miner. J.*, 1972, **6**, 433–441.
17. Shevchenko, A. V., Lopato, L. M., Maister, I. M. and Gorbunov, O. S., *Russ. J. Inorg. Chem. (Engl. Transl.)*, 1980, **25**, 1379–1381.
18. McHale, A. E. and Roth, R. S., Low-temperature phase relationships in the system ZrO_2–TiO_2. *J. Am. Ceram. Soc.*, 1986, **69**, 827–832.
19. Troitzsch, U. and Ellis, D., The ZrO_2–TiO_2 phase diagram. *J. Mater. Sci.*, 2005, **40**, 4571–4577.
20. Hom, B. K., Stevens, R., Woodfield, B. F., Boerio-Goates, J., Putnam, R. L., Helean, K. B. and Navrotsky, A., The thermodynamics of formation, molar heat capacity, and thermodynamic functions of $ZrTiO_4$ (cr). *J. Chem. Thermodyn.*, 2001, **33**, 165–178.
21. Bordet, P., McHale, A. E., Santoro, A. and Roth, R. S., Powder neutron diffraction study of $ZrTiO_4$, $Zr_5Ti_7O_{24}$, and $FeNb_2O_6$. *J. Solid State Chem.*, 1986, **64**, 30–46.
22. Sham, E. L., Aranda, M. A. G., Farfan-Torres, E. M., Gottifredi, J. C., Martinez-Lara, M. and Bruque, S., Zirconium titanate from sol–gel synthesis: thermal decomposition and quantitative phase analysis. *J. Solid State Chem.*, 1998, **139**, 225–232.
23. Troitzsch, U., Christy, A. G. and Ellis, D. J., The crystal structure of disordered $(Zr,Ti)O_2$ solid solution including srilankite: evolution towards tetragonal ZrO_2 with increasing Zr. *Phys. Chem. Miner.*, 2005, **32**, 504–514.
24. Christoffersen, R. and Davies, P. K., Structure of commensurate and incommensurate ordered phases in the system $ZrTiO_4$–$Zr_5Ti_7O_{24}$. *J. Am. Ceram. Soc.*, 1992, **75**, 563–569.

25. Park, Y., Thermal expansion and cooling rate dependence of transition temperature in $ZrTiO_4$ single crystal. *Mater. Res. Bull.*, 1998, **33**, 1325–1329.
26. Troitzsch, U., Christy, A. G. and Ellis, D. J., Synthesis of ordered ziconium titanate $(Zr,Ti)_2O_4$ from the oxides using fluxes. *J. Am. Ceram. Soc.*, 2004, **87**, 2058–2063.
27. Mizutani, N., Tajima, Y. and Kato, M., Phase relations in the system Y_2O_3–TiO_2. *J. Am. Ceram. Soc.*, 1976, **59**, 168.
28. Michel, D., Perez y Jorba, M. and Collongues, R., Etude de la Transformation Ordre-Désordre de la Structure Fluorite à la Structure Pyrochlore pour des Phases $(1-x)\,ZrO_2 - x\,Ln_2O_3$. *Mater. Res. Bull.*, 1974, **9**, 1457–1468.
29. Shamrai, G. V., Magunov, R. L., Stasenko, I. V. and Zhirnova, A. P., The Dy_2O_3–TiO_2 system. *Inorg. Mater. (Engl. Transl.)*, 1989, **25**, 233–235.
30. Waring, J. L. and Schneider, S. J., Phase equilibrium relationships in the system Gd_2O_3–TiO_2. *J. Res. Natl. Bur. Stand.*, 1965, **69A**, 255–261;
Yokokawa, H., Sakai, N., Kawada, T. and Dokiya, M., Phase diagram calculations for ZrO_2 based ceramics: thermodynamic regularities in zirconate formation and solubilities of transition metal oxides. In *Science and Technology of Zirconia V*, ed. S. S. S. Badwal, M. J. Bannister and R. H. J. Hannik. Technomic Publishing Co. Inc., Lancaster, PA, 1993, pp. 59–68.
31. Feighery, A. J., Irvine, J. T. S., Fagg, D. P. and Kaiser, A., Phase relations at 1500 °C in the ternary system ZrO_2–Y_2O_3–TiO_2. *J. Solid State Chem.*, 1999, **143**, 273–276.
32. Kobayashi, K., Kato, K., Terabe, K., Yamaguchi, S. and Iguchi, Y., Phase relation of ZrO_2–$YO_{1.5}$–TiO_2 ceramics prepared by sol–gel method. *J. Ceram. Soc. Jpn.*, 1998, **105**, 860–865.
33. Colomer, M. T., Duran, P., Caballero, A. and Jurado, J. R., Microstructure, electrical properties and phase equilibria relationships in the ZrO_2–Y_2O_3–TiO_2 system: the subsolidus isothermal section at 1500 °C. *Mater. Sci. Eng.*, 1997, **A229**, 114–122.
34. Duran, P., Capel, F., Moure, C., González-Elipe, A. R., Caballero, A. and Bañares, M. A., Mixed (oxygen ion and n-type) conductivity and structural characterization of titania-doped stabilized tetragonal zirconia. *J. Electrochem. Soc.*, 1999, **146**, 2425–2434.
35. Schaedler, T. A., Girma, S., Gandhi, A. S., Sampath, S. and Levi, C. G., Metastable phase evolution in TiO_2–$YO_{3/2}$–ZrO_2. *Mater. Res. Soc. Symp. Proc.*, Vol. 835, Warrendale, PA, 2005, pp. 69–74.
36. Andresson, J.-O., Helander, T., Höglund, L., Shi, P. and Sundman, B., THERMO-CALC & DICTRA, computational tools for materials science. *CALPHAD*, 2002, **26**, 273–312.
37. Saunders, N. and Miodovnik, P., *CALPHAD (Calculation of Phase Diagram: a Comprehensive Guide)*. Pergamon, Oxford, 1998.
38. Hillert, M., The compound energy formalism. *J. Alloys Compd.*, 2001, **320**, 161–176.
39. Fabrichnaya, O., Wang, C., Zinkevich, M., Levi, C. G. and Aldinger, F., Phase equilibria and thermodynamic properties of the ZrO_2–$GdO_{1.5}$–
$YO_{1.5}$ system. *J. Phase Equilib. Diffus.*, 2005, **26**, 591–604.
40. Helean, K. B., Ushakov, S. V., Brown, C. E., Navrotsky, A., Lian, J., Ewing, R. C., Farmer, J. M. and Boatner, L. A., Formation enthalpies of rare earth titanate pyrochlores. *J. Solid State Chem.*, 2004, **177**, 1858–1866.
41. Cancarevic, M., Zinkevich, M. and Aldinger, F., Thermodynamic assessment of the PZT system. *J. Ceram. Soc. Jpn.*, 2006, **114**, 937–949.
42. Li, P., Chen, I. and Penner-Hahn, J. E., Effects of dopants on zirconia stabilization—an X-ray absorption study. II. Tetravalent dopants. *J. Am. Ceram. Soc.*, 1994, **77**, 1281–1288.
43. Gallardo-López, A., Martínez-Fernández, J., Domínguez-Rodríguez, A. and Ernst, F., Origin of diffuse electron scattering in yttria-cubic-stabilized zirconia single crystals with 24–32 mol% yttria. *Philos. Mag. A*, 2001, **81**, 1675–1689.
44. Liu, Y., Withers, R. L. and Noren, L., The pyrochlore to 'defect fluorite' transition in the $Y_2(Zr_yTi_{1-y})_2O_7$ system and its underlying crystal chemistry. *J. Solid State Chem.*, 2004, **177**, 4404–4412.